Original Research

SPINE RESEARCH

OPEN

Biomechanical characteristics of first coronal reverse vertebrae in degenerative lumbar scoliosis

A study using finite element analysis

Zhenguo Shang[a], Di Zhang[a], Yanhong Wang[b], Zhiyong Hou[c], Jiaxin Xu[a], Hengrui Chang[a], Hui Wang[a,*]

Abstract

Background: Whether the first coronal reverse vertebrae (FCRV) can directly cause biomechanical changes in adjacent segments remains unclear.

Objective: This study aimed to explore the biomechanical changes in adjacent discs of FCRV to better understand the stress distribution of degenerative lumbar scoliosis.

Methods: According to the plain computed tomography scan data of the T11–L1 segment of a degenerative lumbar scoliosis patient, T12 was the FCRV, and a 3-dimensional finite element model was established accurately. The T11–12 segment disc was defined as the adjacent upper disc (UD), axial section as half of the UD. Similarly, T12–L1 disc was the adjacent lower disc (LD), axial section as half of the LD. The biomechanical changes in adjacent discs of the FCRV under different loads were assessed.

Results: Rotational load was the highest under different loads, but it is usually instantaneous. It was noted that the LD was subjected to significantly greater stress magnitudes under neutral standing. Although the adjacent discs of the FCRV did not differ significantly with regard to shear stress, a striking difference was noted when the concave and convex sides were considered individually. The concave sides of the adjacent disc were subjected to greater stress under the neutral standing or lateral bending compared with the convex side. Furthermore, the concave sides of the UD, half of the UD (HUD), and HLD were subjected to significantly greater stress under the neutral standing compared with the convex side.

Conclusions: The distal adjacent disc of the FCRV may be at greater risk of degeneration because of taking on more force. These findings can contribute to further treatment planning for the patient and aid physicians' management decision-making.

Abbreviations: FCRV first coronal reverse vertebrae, DLS = degenerative lumbar scoliosis, UD = upper disc, HUD = half of the upper disc, LD = lower disc, HLD = half of the lower disc, FE = finite element, LLB = left lateral bending, RLB = right lateral bending, LAR = left axial rotation, RAR = right axial rotation, NS= neutral standing

Keywords: adjacent disc stress, degenerative lumbar scoliosis, finite element analysis, first coronal reverse vertebrae

1. Introduction

Degenerative lumbar scoliosis (DLS) is a primary coronal plane deformity characterized by a Cobb angle of >10° that develops after skeletal maturity and results from asymmetric intervertebral disc and facet joint degeneration,[1,2] which is of growing interest in health care. Studies have shown that the disorder accounts for 8.85% in Western countries and 13.3% in the Han Chinese population, with a mean age at presentation of 70.5 years.[3–5] It has a substantially debilitating effect on patients' general health,[6] such as pain, stiffness, and loss of function.

ZS, DZ, YW, and ZH contributed to this article equally.

[a] Department of Spinal Surgery, Hebei Medical University Third Hospital, Shijiazhuang, Hebei, China, [b] Department of Orthopaedic Surgery, The People's Hospital of Xingtai, Hebei Medical University, Xingtai, Hebei, China, [c] Department of Orthopaedic Surgery, Hebei Medical University Third Hospital, Shijiazhuang, Hebei, China.

* Correspondence: Hui Wang, Department of Spinal Surgery, Hebei Medical University Third Hospital, 139 Ziqiang Road, Shijiazhuang 050051, Hebei, China (e-mail: hbmuwanghui@hebmu.edu.cn).

Spine Research (2025) 1:3;136–146

Received: 14 February 2025 / Accepted: 18 June 2025

http://dx.doi.org/10.1097/br9.0000000000000007

First coronal reverse vertebrae (FCRV) is defined as the first vertebra that presents an opposite orientation of asymmetric Hounsfield unit ratio compared with the other vertebrae within the major curve.[7] Notably, our previous work demonstrated that the FCRV could be a more reliable selection criterion for the upper instrumented vertebra in patients with DLS.[8,9] Therefore, it is reasonable to believe that the biomechanical effects of the FCRV on adjacent discs are significantly different, but it has never been proved. In recent years, the finite element (FE) methodology has been further developed in the field of scoliosis and has been applied in clinical research and spinal correction procedures. It has important academic significance and application values in determining the etiology, preventing and treating scoliosis, and predicting the progression of the deformity while reducing postoperative complications.[10,11]

In 2015, Zheng et al.[12] built the 3-dimensional FE model of degenerative scoliosis, which was reliable and effective for further biomechanical study of scoliosis. In 2017, Xu et al.[13] investigated the effect of the DLS on the vibrational characteristics of spines, and their findings suggested that DLS could potentially lead to further scoliotic deformity in the spine. In 2019, Haddas et al.[14] found scoliotic spine presented abnormal and asymmetrical kinetic and kinematic behavior using FE models and concluded that a posterior fusion had a large effect on pressure and forces at the adjacent level. Additionally, in 2023, Stott and Driscoll[15] demonstrated that the FE models with excessive curvature might be subjected to greater stress magnitudes, while the straighter spine models might reduce these stresses.

However, although various FE models were reported for spinal deformities, little attention has been paid to the biomechanical characteristics of FCRV in DLS. The purpose of this study is to explore the biomechanical changes in adjacent discs of the FCRV using FE methods to better understand the force of DLS. It lays a foundation for further physical therapy and enhancing long-term surgical outcomes.

2. Materials and methods

2.1. Data acquisition

This study was completed with the knowledge of the subject and was supported by the Institutional Ethics Committee of Hebei Medical University Third Hospital (KS2022-040-1). The data were obtained from a 72-year-old female patient who weighed 70 kg, with the coronal Cobb angle of 41.3°. According to the DLS diagnostic criteria, the scoliosis was diagnosed as DLS. Using a computed tomography (CT) (Siemens, Munich, Germany), transverse scanning was done on the thoracolumbar segment from T10 to S1 in 0.75 mm slices. A 3-dimensional (3D) model of the thoracolumbar spine (T10–S1) was constructed from the CT images using Mimics 20.0 (Materialise, Leuven, Belgium) in this study, shown in Figure 1.

2.2. Building of the 3-dimensional solid model

The detailed steps for building a deformed FE model were obtained from previous research.[12,16,17] Briefly, the geometric information of the thoracolumbar spine (T10–S1) segment was obtained using a CT scan. The CT data was imported into Mimics 20.0 to conduct image segmentation.

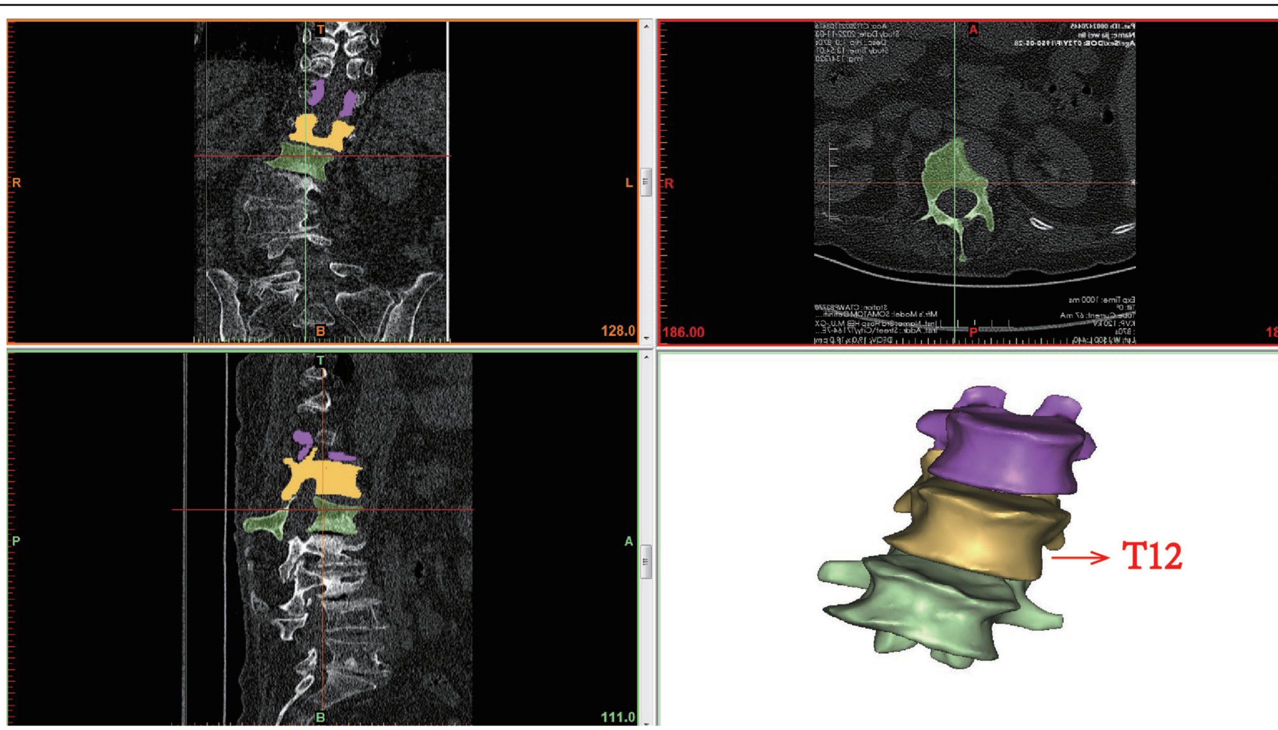

Figure 1. Construction of a 3D model of lumbar spine using computed tomography scan data. Segmentation in 3 different planes, that is, sagittal, coronal, axial, and 3D model are shown.

Geometric model reconstruction was then completed using Geomagic Studio 2013 (Geomagic, Inc., Research Triangle Park, NC, USA). The mesh of each component was created in ABAQUS 2016 (Simulia Inc., USA). The final model was then created using commercial FE software (Abaqus 6.11; Dassault Systemes Simulia Corporation, Pennsylvania).

In this study, the T11–L1 segments of the spine model were selected as our research model, and T12 was the first coronal reverse vertebra. The length of the mesh was designated as 0.5 mm. Cartilage, bone, and other tissues were meshed tetrahedral solid units. According to the physiological anatomical model of the spine, the vertebral body and the intervertebral joint will slide under a certain load, and the friction coefficient was determined to be 0.2. The nucleus pulposus and the annulus fibrosis of the intervertebral disc will not be separated under the load in this study.

The model includes cortical bone and cancellous bone of the vertebral body, fibrous annulus of intervertebral disc, nucleus pulposus, and superior and inferior articular process cartilage and 6 groups of major ligaments of thoracolumbar vertebrae. Bony structures and intervertebral discs are simulated as isotropic elastic materials, and these ligaments, including the anterior longitudinal ligament, posterior longitudinal ligament, ligamentum flavum, intertransverse ligament, supraspinous ligament, and interspinous ligament, were simulated as spring elements.[18] Different materials were distinguished according to the difference of elastic modulus and Poisson ratio. The material properties of bone, ligament, and intervertebral disc were determined by experimental literature,[19,20] and the material attributes and cross-sectional area are shown in Table 1.

2.3. Feasibility validation

Compared with the patient's CT image, we demonstrated that the established FE model was geometrically similar to the object of study. The credibility of the model was verified based on the degree of coincidence between the 2 angles,[10,12] which include coronal Cobb angle and lordosis angle. Although the normal spine verification method was not suitable for scoliosis modeling, geometric variation between the events was negligible. Subsequently, each vertebra was divided into 2 equal parts (upper and lower), and each of which was divided into 5 equal parts (U1 through U5, and L1 through L5, respectively) from the right (concave side) to the left (convex side). Similarly, each disc was divided into 5 equal parts (D1 through D5) from the right side to the left. We set the vertebrae and discs with different elastic modulus, respectively, depending on the Hounsfield gray value based on the CT images.

2.4. Boundary and loading conditions

The moments in this study were referred to Yamamoto et al.'s[21] in vitro test loads. Therefore, 5 Nm moments loading[15,17] and bounding conditions were applied as provided in Yamamoto et al.'s study. The 5 loads in this study simulated the 5 different motion states of the thoracic spine. Under physiological conditions, T11 vertebral body was axially loaded with 450 N. A boundary was applied to constrain the displacement and rotation of all nodes on the base of the L1 vertebral body in all directions. This was also performed to apply a moment of 5 Nm in the axial and sagittal on the upper surface of the T11 vertebral body to simulate left and right bending, left and right rotation.

2.5. Statistical analysis

Statistical analysis was performed using SPSS 26.0 (SPSS Inc., Chicago). A paired t test was employed to evaluate differences between the convex and concave sides, and 1-way analysis of variance was used to analyze the difference of convex or concave sides for biomechanical parameters. In case the difference between paired data or raw data did not follow a normal distribution, the Wilcoxon signed-rank test was performed. Differences were considered to be significant when $p < 0.05$.

3. Results

3.1. FE model

As mentioned previously, the aim of this work was to explore the biomechanical changes in adjacent discs of the FCRV using FE methods to better understand the force of DLS. A 3-dimensional FE model of the T11–L1

Table 1

Material parameters of the FE spinal model.

	Young modulus (MPa)	Poisson ratio	Cross-sectional area (mm^2)
Cortical bone	12,000	0.3	—
Cancellous bone	100	0.3	—
Annulus fibrosis	4.2	0.453	—
Nucleus pulposus	1	0.499	—
Anterior longitudinal ligament	8	0.35	49.1
Posterior longitudinal ligament	10	0.35	22.2
Ligamentum flavum	5	0.35	71.1
Interspinous ligament	5	0.35	49.2
Supraspinous ligament	5	0.35	70.3
Intertransverse ligament	5	0.35	4

FE = finite element.

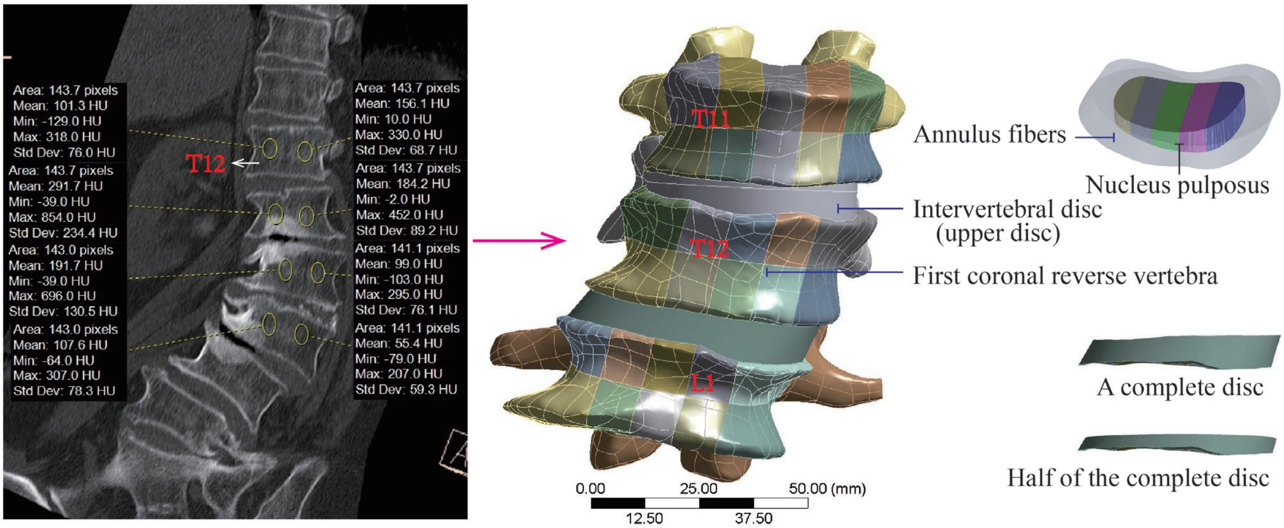

Figure 2. The integral 3-dimensional FE model of DLS, including T11 to L1. DLS = degenerative lumbar scoliosis, FE = finite element.

thoracolumbar spine segments of DLS was constructed in our study, which contained 271,314 elements and 398,724 nodes. The FE model includes finely reconstructed vertebrae, intervertebral discs, ligaments, articular cartilage, and other anatomical structures, and the model is outlined in Figure 2.

Notably, T12 vertebral body was the first coronal reverse vertebra. Depending on the Hounsfield gray value based on the CT images, we set the vertebrae and discs (T11–L1) with different elastic moduli, respectively. For example, the elastic moduli (MPa) of the T12 vertebra from the right (concave side) to the left (convex side), U1 through U5, were 367, 1237, 1410, 1654, and 2523, respectively, and those of L1 through L5 were 576, 1184, 1497, 1549, and 1636, respectively. Additionally, the elastic moduli (MPa) of the T12–L1 segment disc from the right (concave side) to the left (convex side), D1 through D5, were 10.4, 11.1, 11.8, 12.5, and 13.2, respectively. The trend in elastic moduli of the T11–L1 thoracolumbar spine was consistent with the trend in Hounsfield unit.

3.2. Intervertebral disc stress distribution

The T11–12 segment disc was defined as the adjacent upper disc (UD), axial section (at half height of the UD) as half of the UD (HUD). Similarly, the T12–L1 segment disc was defined as the adjacent lower disc (LD), axial section (at half height of the LD) as half of the LD (HLD). Under 450 N vertical downward force and 5 Nm moment loads, this study recorded stress distribution at the surface and axial section of T11–L1 segment discs.

3.3. The maximum von Mises stress values of the intervertebral discs subjected to different loads

Data in Figure 3, for example, show the maximum von Mises stress values at the LD under left lateral bending (LLB), right lateral bending (RLB), left axial rotation (LAR), right axial rotation (RAR), and neutral standing (NS) loads. As can be seen in Figure 4, the maximum von Mises stress values in UD were even higher than those in other discs under the rotational load, which is consistent with results obtained in previous studies.[10] However, although the rotational load was the highest under different loads (Fig. 4), it is usually instantaneous in everyday life, which is consistent with Dubousset's cone of efficiency.[22] It is important to reiterate that the LD was subjected to significantly greater stress magnitudes under the NS.

3.4. Stress distribution at intervertebral discs including LD, HLD, UD, and HUD in lateral bending, axial rotation, and NS

Intervertebral disc shear stresses were investigated at 1 through 9 under each loading condition in the present study. The direction of 1 through 9, the longest line of the coronal plane and evenly spaced, was from the concave side to the convex side in the intervertebral disc. One through 4 were defined as the concave side, and 6 through 9 were defined as the convex side. A negative number indicated a compressive stress and a positive number indicated a tensile stress.

For example, Figure 5 displays that the stress values (1 through 9) at the surface of the LD under the LLB load were 0.00024, 0.000098, 0.00012, 0.00013, 0.00013, 0.00017, 0.00014, 0.0001, and −0.0007 MPa, respectively. Under the RLB load, the stress values of the LD at 1 through 9 were −0.00048, −0.000094, −0.000074, −0.000089, −0.000091, −0.00015, −0.000099, −0.000076, and 0.00097 MPa, respectively. Under the LAR load, the stress values were 0.0023, −0.000081, 0.000016, 0.00011, 0.00025, 0.00031, 0.00028, 0.00028, and 0.00051 MPa, respectively. Under the RAR load, the corresponding values were −0.0015, 0.000079, −0.000013, −0.0001, −0.00024, −0.00031, −0.00028,

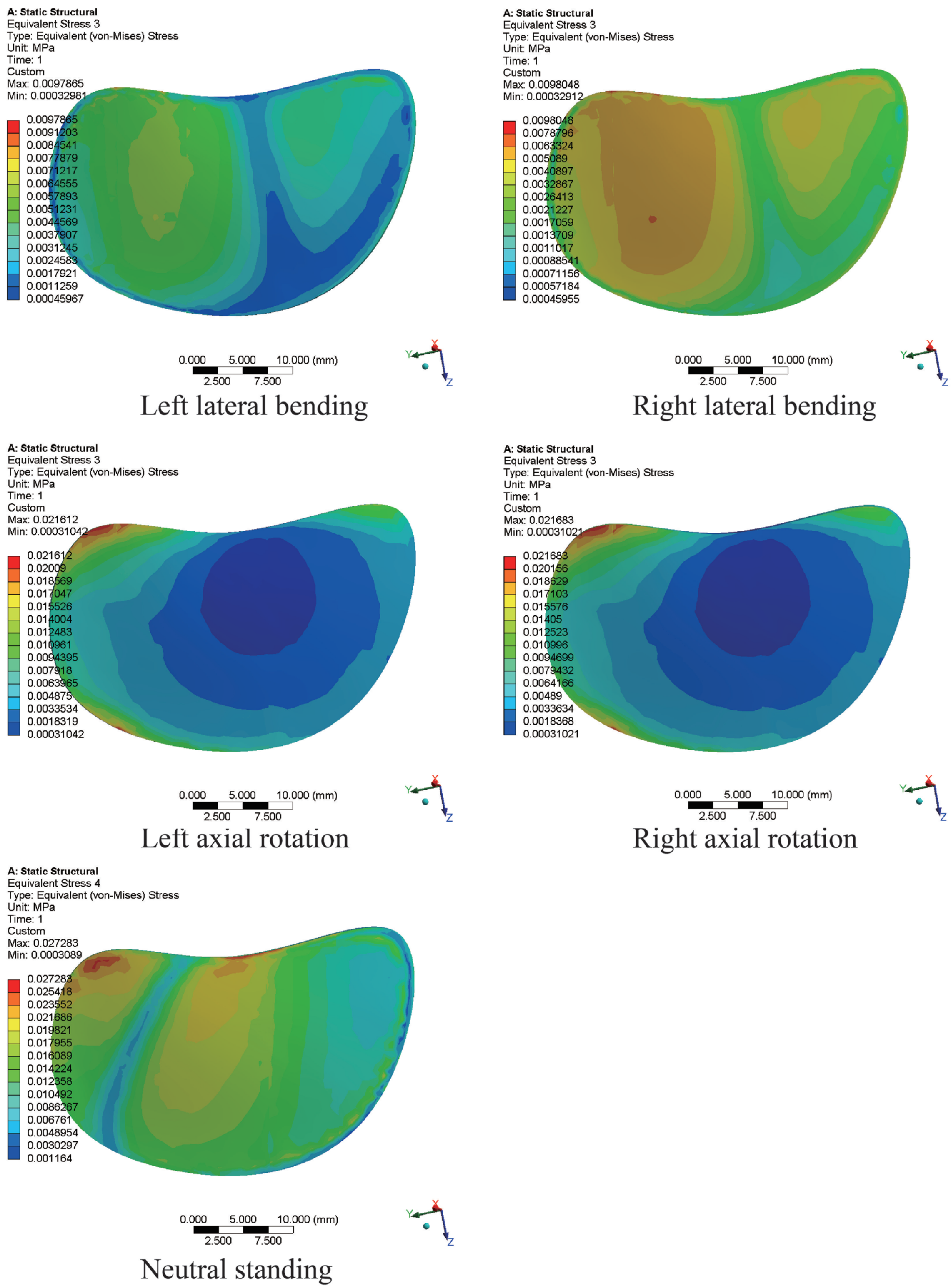

Figure 3. The stress distribution at the adjacent lower disc (LD) in lateral bending (left and right), axial rotation (left and right), and neutral standing in the FE model. FE = finite element.

−0.00027, and −0.00045 MPa, respectively. Under the NS load, the corresponding values were 0.00047, −0.0018, 0.0020, 0.0010, 0.00065, 0.00039, 0.00032, 0.00054, and −0.00043 MPa, respectively.

Interestingly, we found that the intervertebral disc stress under different loads was mainly concentrated on the edge of the intervertebral disc, which is consistent with the results of the FE model established by Chen et al.[23] Additionally, changes in the concave side of LD under the RLB, LAR, RAR, or NS load were dramatic. Moreover, it can be observed from Figure 6 that under the LAR load, the concave and convex sides of UD were both

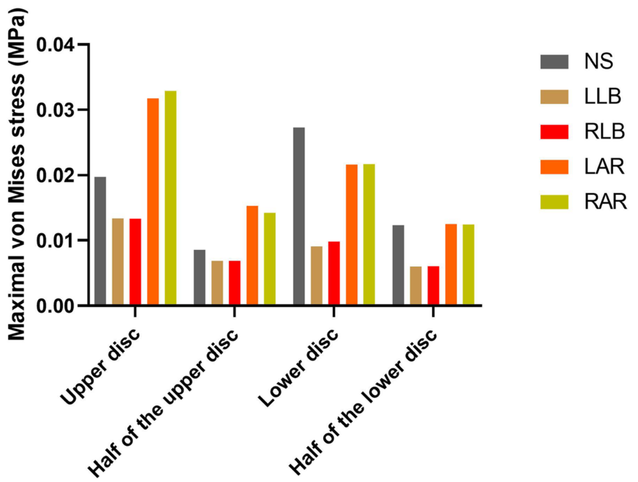

Figure 4. The von Mises stress of the intervertebral discs under various loading conditions for the FE model (T11–L1). FE = finite element, LAR = left axial rotation, LLB = left lateral bending, NS = neutral standing, RAR = right axial rotation, RLB = right lateral bending.

compressed; however, they displayed opposite trends under the RAR load, respectively.

3.5. Shear stress difference between concave and convex disc sides

No significant differences in terms of shear stress were found between UD, HUD, LD, and HLD under different loads (Table 2). However, compared with the convex side, the concave side of the discs of the T11–L1 thoracolumbar spine was subjected to significantly greater stress under the NS, LLB, or RLB load (Table 3). A striking illustration of this can be seen in Table 4 where the concave side of UD was subjected to greater stress magnitudes under the NS load compared with the convex side, and HUD and HLD also displayed similar trends (Tables 4 and 5).

This article contained no information about flexion and extension due to the fact that they significantly affect the anterior and posterior discs rather than the left and right sides.[10] Nevertheless, these results suggest that data obtained using FE model to simulate the force of DLS may further provide strong support for assessing the effect of FCRV on degeneration in adjacent segments in patients with spinal deformity.

4. Discussion

Unlike idiopathic scoliosis, DLS is a chronic condition that results from degenerative bone and soft tissue changes and begins with the intervertebral disc degeneration,[6] and it has a substantially debilitating effect on patients' general health. Disability, pain, and neurological complaints are more commonly reported by DLS patients than cosmetic deformity or curve progression, which are more common complaints among adolescent patients.[24] Intervertebral disc degeneration is a complex and chronic process that begins early in adulthood caused by multiple stresses[25] and involves reduced disc height, loss of water and proteoglycan content, and increased enzymatic degradation.[26]

The degeneration can lead to pathological changes in load-bearing at intervertebral and facet joints, resulting in instability (via rotatory subluxation or olisthesis) and bone remodeling at these joints.[27] Furthermore, a progressive decline in paraspinal and truncal musculature and spinal ligaments is commonly caused by the cycle of remodeling, which ultimately results in spinal deformity. Interestingly, it is often less magnitude, yet it progresses at faster rates.[6]

The results of this FE analysis (FEA) study reveal that FCRV significantly caused changes in the forces on the adjacent intervertebral discs under different loads. Most notably, the LD was subjected to significantly greater stress magnitudes under the NS load. Our findings can contribute to further treatment planning for the patient and aid physicians' management decision-making. For example, proximal fusion level above FCRV might help to prevent postoperative adjacent segment degeneration in patients with DLS. This is the first study, to our knowledge, to investigate the biomechanical characteristics of FCRV in patients with DLS.

The FEA has been further developed in the field of scoliosis and can provide strong support for clinical research due to its good predictive ability and without any harm to the patient. For example, it can be used for the prevention and diagnosis of spinal deformity, assist in surgery, and help in the design of curative effects and evaluation.[28] In addition, numerical experiments are less costly and more efficient compared with in vitro specimen experiments, and the experimental conditions, such as material properties, are freely controlled based on spinal anatomy.[12,29] In this study, the FE model simulated the combined effects of different morphological, structural changes and changes to the material properties of spinal scoliosis. Through FEA, the results of any biomechanical changes in the thoracolumbar spine, similar to actual anatomical situations, can be accurately recorded.

We found that the rotational load was the highest under different loads, which is consistent with results obtained in previous studies.[10] However, axial rotation is usually instantaneous in everyday life, which is consistent with Dubousset's cone of efficiency.[22] It is important to reiterate that the LD was subjected to significantly greater stress magnitudes under the NS. These findings extend our previous study, confirming that the distal adjacent segment of the FCRV is more likely to be injured because of greater stress than the proximal adjacent segment.[8] The main reason is that scoliosis changes the normal shape of the spine and may not effectively transfer the load downward. Additionally, Krismer et al.[30] reported that fissure formation of the annulus in the degenerated disc was associated with torsion. Thus, the stress increases probably accelerated fissure formation of the

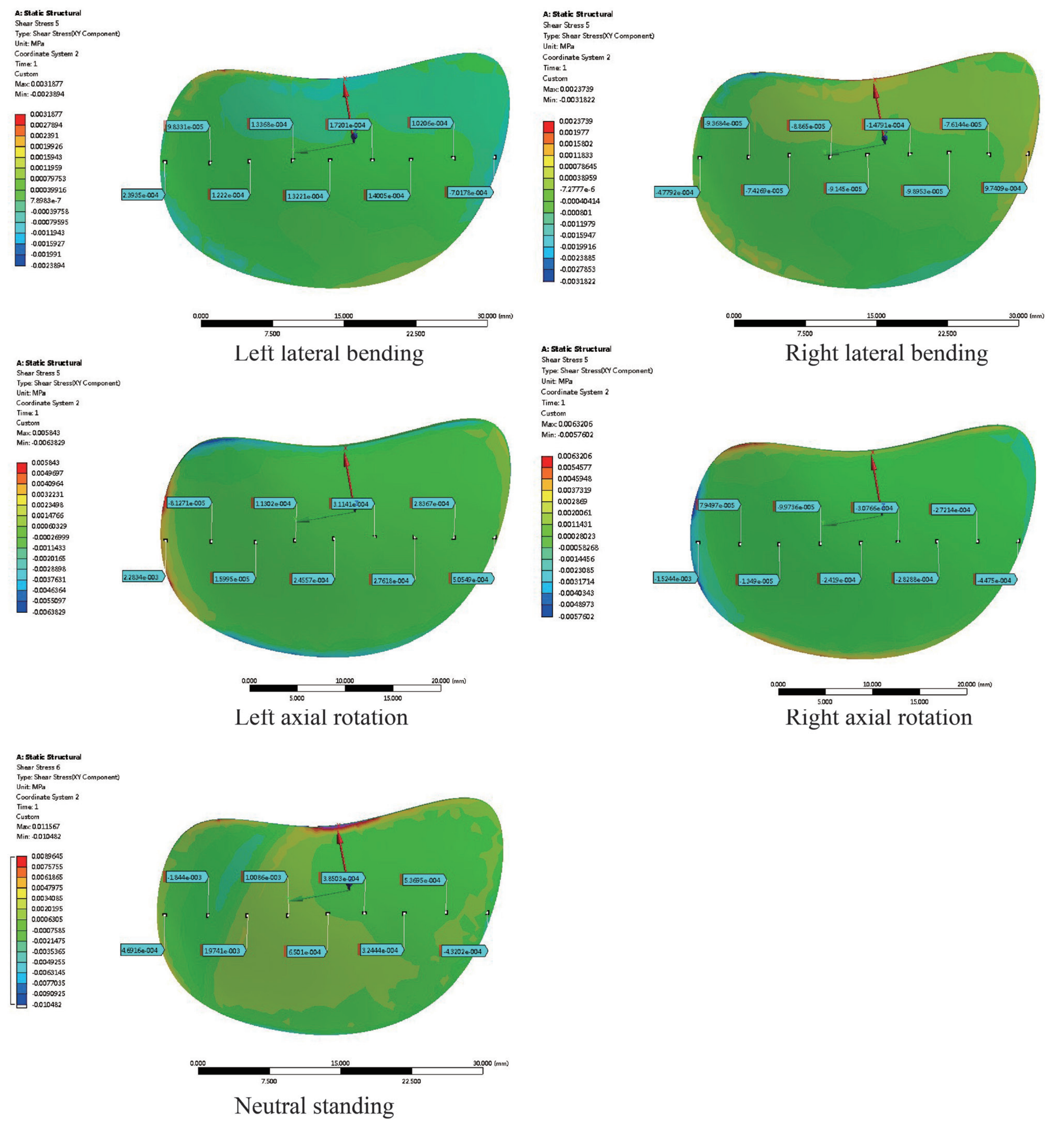

Figure 5. Shear stress of the adjacent lower disc in various postures, including lateral bending, axial rotation, and neutral standing.

disc in torsion. The stress showed a sharp increase in the intervertebral discs during axial rotation, and it was likely to cause the disc early degeneration change.[31] Therefore, patients with DLS should avoid excessive overload-bearing and frequent axial rotations of the spine.

In our study, the intervertebral disc stress under different loads was mainly concentrated on the edge of the intervertebral disc, which is consistent with the results of the FE model established by Chen et al.[23] However, this study demonstrated that the concave side of the discs was subjected to significantly greater stress under the NS, LLB, or RLB load. One could predict that the stress concentration would be enhanced by a tremendous alteration of different elastic moduli. Therefore, patients with DLS should also avoid lateral bending and excessive weight bearing, which can cause injury to the intervertebral disc.[32] This may be due to increased differences in elastic modulus (MPa) between the concave and convex sides of the FCRV.

Incorrect posture could lead to different stress load changes, which might be a potential risk factor for the development or progression of DLS. However, it is still unclear whether incorrect body posture is directly associated with scoliosis.[33] We posit that thoracolumbar

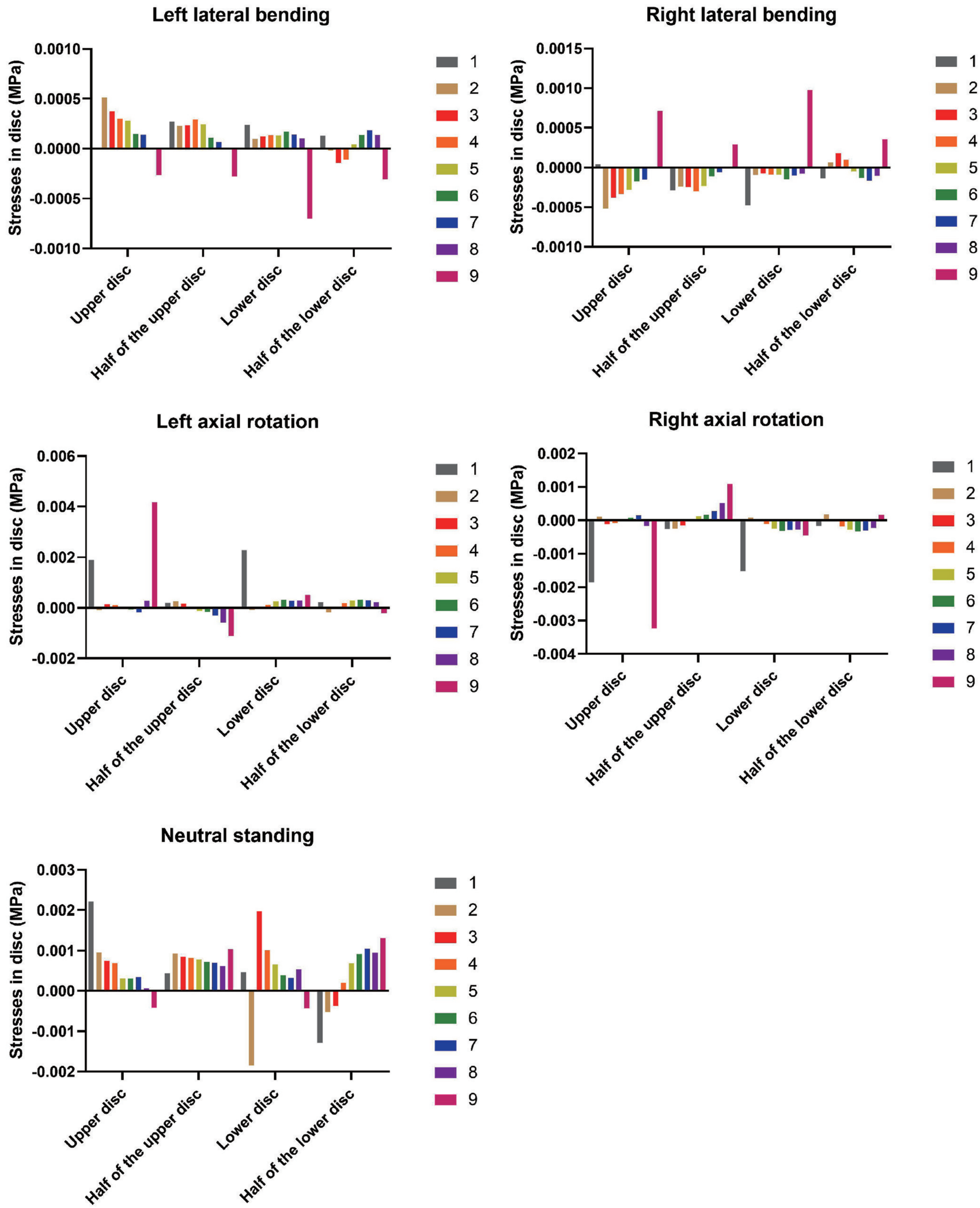

Figure 6. Effect of various postures on intervertebral discs for the FE model (T11–L1). FE = finite element.

concavity was associated with AIS, similar to the trends observed in the lumbar concavity.[34] We speculate that this mechanism also operates in DLS. There is no denying that some postures will affect the spine and intervertebral discs in everyday life. For example, when the body posture bends to the concave side, the pressure on the concave side of the thoracolumbar spine is further increased, which has an adverse effect on the thoracolumbar spine. Guy and Aubin[35] reported that the full brace-wear compliance scenarios resulted 31/35 (89%)

Table 2

The FE results in the discs of the T11–L1 thoracolumbar spine of DLS subjected to different loads.

	LLB	RLB	NS	LAR	RAR
UD	0.0002 ± 0.0002	−0.0001 ± 0.0004	0.0003 ± 0.0017	0.0007 ± 0.0014	−0.0006 ± 0.0012
HUD	0.0001 ± 0.0002	−0.0001 ± 0.0002	0.0003 ± 0.0012	−0.0002 ± 0.0004	0.0002 ± 0.0004
LD	0.00005 ± 0.0003	−0.00002 ± 0.0004	0.0005 ± 0.0003	0.0004 ± 0.0007	−0.0003 ± 0.0005
HLD	0.000006 ± 0.0002	−0.00001 ± 0.0002	0.0001 ± 0.0009	0.0001 ± 0.0002	−0.0001 ± 0.0002
F	0.987	0.513	0.164*	1.856*	1.959
p value	0.411	0.677	0.920	0.157	0.140

Analysis of variance was performed, significant if $p < 0.05$.
DLS = degenerative lumbar scoliosis, FE = finite element, HLD = half of the lower disc, HUD = half of the upper disc, LAR = left axial rotation, LD = lower disc, LLB = left lateral bending, NS = neutral standing, RAR = right axial rotation, RLB = right lateral bending, UD =upper disc.
*Welch's test.

Table 3

The FE results in the convex and concave sides of the T11–L1 thoracolumbar spine of DLS subjected to different loads.

	LLB	RLB	NS	LAR	RAR
Concave side	0.0002 ± 0.0002	−0.0002 ± 0.0002	0.0011 ± 0.0009	0.0003 ± 0.0007	−0.0003 ± 0.0006
Convex side	−0.00001 ± 0.0002	0.0001 ± 0.0003	−0.0005 ± 0.0008	0.0003 ± 0.0011	−0.0002 ± 0.0009
t	2.351	−2.455	5.597	0.203	−0.251
p value	0.033	0.027	0.000	0.841	0.805

A paired *t* test was performed; significance was set at $p < 0.05$.
DLS = degenerative lumbar scoliosis, FE = finite element, LAR = left axial rotation, LLB = left lateral bending, NS = neutral standing, RAR = right axial rotation, RLB = right lateral bending.

Table 4

The FE results in the convex and concave sides of the T11–12 thoracic spine of DLS subjected to different loads.

	Upper disc			Half of the upper disc		
	Convex side	Concave side	*p* value	Convex side	Concave side	*p* value
LLB	0.000007 (0.0002)	0.0003 (0.0002)	0.156	−0.00002 (0.0002)	0.0003 (0.00003)	0.065
RLB	0.0001 (0.0004)	−0.0003 (0.0002)	0.223	0.00003 (0.0002)	−0.0003 (0.00003)	0.055
LAR	0.0011 (0.0021)	0.0005 (0.0009)	0.695	−0.0005 (0.0004)	0.0001 (0.0001)	0.023
RAR	−0.0008 (0.0016)	−0.0005 (0.0009)	0.785	0.0005 (0.0004)	−0.0002 (0.0001)	0.019
NS	−0.0011 (0.0006)	0.0018 (0.0013)	0.006	−0.0007 (0.0005)	0.0014 (0.0010)	0.009

A paired *t* test was performed, significant if $p < 0.05$.
DLS = degenerative lumbar scoliosis, FE = finite element, LAR = left axial rotation, LLB = left lateral bending, NS = neutral standing, RAR = right axial rotation, RLB = right lateral bending.

Table 5

The FE results in the convex and concave sides of the T12–L1 thoracolumbar spine of DLS subjected to different loads.

	Lower disc			Half of the lower disc		
	Convex side	Concave side	*p* value	Convex side	Concave side	*p* value
LLB	−0.00007 (0.0004)	0.0001 (0.00006)	0.364	0.00004 (0.0002)	−0.00003 (0.0001)	0.552
RLB	0.0002 (0.0005)	−0.0002 (0.0002)	0.262	−0.00001 (0.0002)	0.00005 (0.0001)	0.646
LAR	0.0003 (0.0001)	0.0006 (0.0011)	0.708	0.0002 (0.0002)	0.00006 (0.0002)	0.627
RAR	−0.0003 (0.00008)	−0.0004 (0.0008)	0.883	−0.0002 (0.0002)	−0.00003 (0.0002)	0.485
NS	0.0004 (0.0003)	0.0005 (0.0003)	0.700	−0.0008 (0.0007)	0.0009 (0.0003)	0.003

A paired *t* test was performed, significant if $p < 0.05$.
DLS = degenerative lumbar scoliosis, FE = finite element, LAR = left axial rotation, LLB = left lateral bending, NS = neutral standing, RAR = right axial rotation, RLB = right lateral bending.

simulated spine deformities progressing by < 5° over 2 years of treatment. These studies support our conclusion. Our results provide compelling evidence that the biomechanical effects of the FCRV on adjacent discs are significantly different, which has direct clinical guiding implications.

However, some limitations are worth noting: Although our hypotheses were supported statistically, the sample was not reassessed once the program was over. The FE model of the test is the thoracolumbar spine, which mainly does not combine the cervical and lumbar segments to analyze the effect of the spine load. The test model only analyzes the stress in the intervertebral discs but does not consider the condition of muscle load, and ligaments were modeled as a 1-dimensional nonlinear spring element. Therefore, the model was only able to reflect trends in the response of the FCRV under different loads and could not fully represent actual values. However, this study will be beneficial in our understanding of the stress characteristics of DLS, and it lays a foundation for further physical therapy and surgical concerns about posture correction. Future research should attempt to measure these variables using experimental methods and apply them to the validation of the FE model.

5. Conclusions

FCRV represents the transitional point of the mechanical load on the coronal plane, which caused the LD to take on greater stress magnitudes, notably under the NS. The stress demonstrated local concentration, particularly on the concave side of the scoliosis. These findings could contribute to further treatment planning for the patient by providing computer-aided assessments to aid physicians' management decision-making.

Acknowledgments

The authors declare that there are no acknowledgments.

Ethical statement

Approval was granted by the Ethics Committee of the Third Hospital of Hebei Medical University (KS2022-040-1), Shijiazhuang 050051, Hebei, China. The patient provided informed consent to allow her information to be used for research purposes.

Conflicts of interest

The authors have no conflicts of interest to disclose.

Funding source

This research was supported by the Natural Science Foundation of Hebei Province (No. H2022206056) and Major Science and Technology Projects of Hebei Province (22377707D).

Data availability statement

The raw data supporting the conclusions of this article are available from the authors upon reasonable request.

Author contributions

Study design: Hui Wang.
Software, validation: Zhenguo Shang, Di Zhang, Yanhong Wang, and Zhiyong Hou.
Data measurements and analysis: Jiaxin Xu and Hengrui Chang.
Writing the manuscript: Zhenguo Shang.
Manuscript revision, formal analysis: Zhiyong Hou.
Read and approved the final manuscript: Hui Wang.

References

[1] Aebi M. The adult scoliosis. Eur Spine J. 2005;14:925–48.
[2] Kotwal S, Pumberger M, Hughes A, Girardi F. Degenerative scoliosis: a review. HSS J. 2011;7:257–64.
[3] Xu L, Sun X, Huang S, et al. Degenerative lumbar scoliosis in Chinese Han population: prevalence and relationship to age, gender, bone mineral density, and body mass index. Eur Spine J. 2013;22:1326–31.
[4] Kebaish KM, Neubauer PR, Voros GD, Khoshnevisan MA, Skolasky RL. Scoliosis in adults aged forty years and older: prevalence and relationship to age, race, and gender. Spine (Phila Pa 1976). 2011;36:731–6.
[5] Grubb SA, Lipscomb HJ, Coonrad RW. Degenerative adult onset scoliosis. Spine (Phila Pa 1976). 1988;13:241–5.
[6] Diebo BG, Shah NV, Boachie-Adjei O, et al. Adult spinal deformity. Lancet. 2019;394:160–72.
[7] Wang H, Zou D, Sun Z, Wang L, Ding W, Li W. Hounsfield unit for assessing vertebral bone quality and asymmetrical vertebral degeneration in degenerative lumbar scoliosis. Spine (Phila Pa 1976). 2020;45:1559–66.
[8] Wang H, Sun Z, Wang L, Zou D, Li W. Proximal fusion level above first coronal reverse vertebrae: an essential factor decreasing the risk of adjacent segment degeneration in degenerative lumbar scoliosis. Global Spine J. 2023;13:149–155.
[9] Hou X, Sun Z, Li W, et al. Upper instrumented vertebrae selection criteria for degenerative lumbar scoliosis based on the Hounsfield unit asymmetry of the first coronal reverse vertebrae: an observational study. J Orthop Surg Res. 2023;18:819.
[10] Zhang Q, Chon T, Zhang Y, Baker JS, Gu Y. Finite element analysis of the lumbar spine in adolescent idiopathic scoliosis subjected to different loads. Comput Biol Med. 2021;136:104745.
[11] Kamal Z, Rouhi G. Significance of spine stability criteria on trunk muscle forces following unilateral muscle weakening: a comparison between kinematics-driven and stability-based kinematics-driven musculoskeletal models. Med Eng Phys. 2019;73:51–63.
[12] Zheng J, Yang Y, Lou S, Zhang D, Liao S. Construction and validation of a three-dimensional finite element model of degenerative scoliosis. J Orthop Surg Res. 2015;10:189.
[13] Xu M, Yang J, Lieberman I, Haddas R. Finite element method-based study for effect of adult degenerative scoliosis on the spinal vibration characteristics. Comput Biol Med. 2017;84:53–8.
[14] Haddas R, Xu M, Lieberman I, Yang J. Finite element based-analysis for pre and post lumbar fusion of adult degenerative scoliosis patients. Spine Deform. 2019;7:543–52.
[15] Stott B, Driscoll M. Biomechanical evaluation of the thoracolumbar spine comparing healthy and irregular thoracic and lumbar curvatures. Comput Biol Med. 2023;160:106982.
[16] Cai XY, Sang D, Yuchi CX, et al. Using finite element analysis to determine effects of the motion loading method on facet joint forces after cervical disc degeneration. Comput Biol Med. 2020;116:103519.

[17] Biswas JK, Rana M, Malas A, Roy S, Chatterjee S, Choudhury S. Effect of single and multilevel artificial inter-vertebral disc replacement in lumbar spine: a finite element study. Int J Artif Organs. 2022;45:193–199.
[18] Du C, Mo Z, Tian S, et al. Biomechanical investigation of thoracolumbar spine in different postures during ejection using a combined finite element and multi-body approach. Int J Numer Method Biomed Eng. 2014;30:1121–31.
[19] Polikeit A, Ferguson SJ, Nolte LP, Orr TE. Factors influencing stresses in the lumbar spine after the insertion of intervertebral cages: finite element analysis. Eur Spine J. 2003;12:413–20.
[20] Wiczenbach T, Pachocki L, Daszkiewicz K, Łuczkiewicz P, Witkowski W. Development and validation of lumbar spine finite element model. PeerJ. 2023;11:e15805.
[21] Yamamoto I, Panjabi MM, Crisco T, Oxland T. Three-dimensional movements of the whole lumbar spine and lumbosacral joint. Spine (Phila Pa 1976). 1989;14:1256–60.
[22] Dubousset J. Three-dimensional analysis of the scoliotic deformity. In: Weinstein S, ed. The Pediatric Spine: Principles and Practice. Raven Press; 1994:479–96.
[23] Chen CS, Cheng CK, Liu CL, Lo WH. Stress analysis of the disc adjacent to interbody fusion in lumbar spine. Med Eng Phys. 2001;23:483–91.
[24] Bess S, Boachie-Adjei O, Burton D, et al; International Spine Study Group. Pain and disability determine treatment modality for older patients with adult scoliosis, while deformity guides treatment for younger patients. Spine (Phila Pa 1976). 2009;34:2186–90.
[25] Wang F, Cai F, Shi R, Wang X-H, Wu X-T. Aging and age related stresses: a senescence mechanism of intervertebral disc degeneration. Osteoarthritis Cartilage. 2016;24:398–408.
[26] Sampara P, Banala RR, Vemuri SK, Av GR, Gpv S. Understanding the molecular biology of intervertebral disc degeneration and potential gene therapy strategies for regeneration: a review. Gene Ther. 2018;25:67–82.
[27] Sparrey CJ, Bailey JF, Safaee M, et al. Etiology of lumbar lordosis and its pathophysiology: a review of the evolution of lumbar lordosis, and the mechanics and biology of lumbar degeneration. Neurosurg Focus. 2014;36:E1.
[28] Zadpoor AA, Weinans H. Patient-specific bone modeling and analysis: the role of integration and automation in clinical adoption. J Biomech. 2015;48:750–60.
[29] Zhang Y, Awrejcewicz J, Baker JS, Gu Y. Cartilage stiffness effect on foot biomechanics of Chinese bound foot: a finite element analysis. Front Physiol. 2018;9:1434.
[30] Krismer M, Haid C, Behensky H, Kapfinger P, Landauer F, Rachbauer F. Motion in lumbar functional spine units during side bending and axial rotation moments depending on the degree of degeneration. Spine (Phila Pa 1976). 2000;25:2020–7.
[31] Ke S, He X, Yang M, Wang S, Song X, Li Z. The biomechanical influence of facet joint parameters on corresponding segment in the lumbar spine: a new visualization method. Spine J. 2021;21:2112–21.
[32] Langrana NA, Lee CK, Yang SW. Finite-element modeling of the synthetic intervertebral disc. Spine (Phila Pa 1976). 1991;16(6 Suppl):S245–52.
[33] Comité Nacional de Adolescencia SAP; Comité de Diagnóstico por Imágenes SAP; Sociedad Argentina de Ortopedia y Traumatología Infantil; Sociedad Argentina de Patología de la Columna Vertebral (SAPCV); Comité de Diagnóstico por Imágenes; Colaboradores. [Adolescent idiopathic scoliosis]. Arch Argent Pediatr. 2016;114:585–94. Spanish.
[34] Yan B, Lu X, Qiu Q, Nie G, Huang Y. Association between incorrect posture and adolescent idiopathic scoliosis among Chinese adolescents: findings from a large-scale population-based study. Front Pediatr. 2020;8:548.
[35] Guy A, Aubin CE. Finite element simulation of growth modulation during brace treatment of adolescent idiopathic scoliosis. J Orthop Res. 2023;41:2065–74.